scientific reports

Check for updates

OPEN

A high-resolution machine learning and multi-source remote sensing approach for estimating net primary productivity in campus green spaces

Chien-Hao Sung[1], Candera Wijaya[2], Aji Kusumaning Asri[1], Yinq-Rong Chern[1], Tee-Ann Teo[3], Wan-Yu Liu[4,5], Chia-Ho Lee[6], Yu-Liang Hsu[7] & Chih-Da Wu[1,5,7,8,9,10]✉

This research proposes an innovative framework that integrates Machine Learning classification, the Carnegie-Ames-Stanford Approach (CASA), unmanned aerial vehicles (UAV), and multi-source data to estimate the net primary productivity (NPP) of campus green spaces. Green space was extracted using Random Forest with an overall accuracy of 94.6% (Kappa = 0.919). The fraction of Photosynthetically Active Radiation (FPAR) was derived from UAV multispectral vegetation indices, while temperature, solar radiation, and the Water Stress Factor (WSF) estimated from Sentinel 2 imagery were integrated into CASA to model NPP. Validation showed that our approach offered higher R^2 and lower RMSE compared to traditional CASA. Across two seasons, the model achieved R^2 values of 0.68–0.79, with RMSE of 11.74–17.01 $gC \cdot m^{-2} \cdot month^{-1}$ and RRMSE of 15.63–22.65%. Seasonal dynamics and human activities explained the observed variation in R^2, RMSE, and RRMSE. Our scalable approach suggests that campus green spaces have the potential to serve as contributors to urban carbon sinks. This method has strong potential to inform sustainable urban planning, carbon offset programs, and nature-based climate solutions.

Keywords Unmanned Aerial Vehicle (UAV) Multispectral Image, Carnegie-Ames-Stanford Approach (CASA), Random Forest Classification, Urban Green Space, Net Primary Productivity

The urgent need to address climate change has elevated carbon neutrality and net-zero emissions to global priorities. In response, the twenty-first century saw the inception of several critical international projects aimed at addressing these issues. Key international initiatives, such as the REDD + , UN SDGs, and the Paris Agreement, underscore carbon neutrality and net-zero emissions as critical climate actions, a focus reiterated at COP 28 in 2023. These projects highlighted the essential roles of carbon neutrality, carbon sinks, and net-zero emissions in combating climate change. To achieve carbon neutrality, Nature-based Solutions (NBS), solving environmental problems under sustainable management, and leveraging natural processes for sustainable management came into the spotlight[1]. Green space was the most essential element under the concept of NBS for reaching carbon neutrality especially for urban areas[2]. The research underscored the importance of green spaces in achieving carbon neutrality since the forest ecosystem covered one-third of the Earth's land[3–5].

[1]Department of Geomatics, College of Engineering, National Cheng Kung University, Tainan 70101, Taiwan. [2]Agricultural Engineering Research Center, Taoyuan 32061, Taiwan. [3]Department of Civil Engineering, National Yang Ming Chiao Tung University, No. 1001, Daxue Rd., East District, Hsinchu City 300, Taiwan. [4]Department of Forestry, National Chung Hsing University, Taichung City 402, Taiwan. [5]Innovation and Development Center of Sustainable Agriculture, National Chung Hsing University, Taichung City 402, Taiwan. [6]Chiayi City Environmental Protection Bureau, No. 184, Wu Feng North Road, Chiayi City 60045, Taiwan. [7]Department of Architecture, National Cheng Kung University, 1 University Rd., East District, Tainan 701, Taiwan. [8]National Institute of Environmental Health Sciences, National Health Research Institutes, Miaoli 35053, Taiwan. [9]Research Center for Precision Environmental Medicine, Kaohsiung Medical University, Kaohsiung 807, Taiwan. [10]Chronic Diseases and Health Promotion Research Center, Chang Gung University of Science and Technology (CGUST), Chiayi 613, Taiwan. ✉email: chidawu@mail.ncku.edu.tw

Forest carbon storage and sequestration, one of the most essential carbon sinks for NBS, spans multiple systems and scales and relies on two complementary tools, forest inventory and remote sensing. Forest inventory is one of the most foundational tools for estimating carbon stocks at national/regional, urban, and campus levels[6–8]. Forest inventory can also be adopted as the independent variable for forest carbon storage and sequestration modeling[9–11]. Remote sensing, another common tool, depending on the remote sensing platform, extends coverage across scales, enabling consistent and in-time estimation from national to campus levels [9,11–13]. National and regional forest carbon storage and sequestration research typically focuses on establishing long-term baselines and providing policy support[6,12]. Urban forest carbon storage and sequestration research mostly focuses on urban planning decisions and city-scale sustainable development[14]. Campus research primarily focuses on facilities management, with the goal of supporting species diversity and carbon sequestration research[8,15]. The results of national and regional research can reach the Petagram (10^{15} g) scale, while city research reaches the Teragram (10^{12} g) to the Gigagram (10^{9} g). As for the campus research, the most common scale was in Kilograms (10^{3} g) to Megagram (10^{6} g)[6,10,13,14]

Research on fragmented urban green spaces, especially campus green spaces, remains limited and underexplored[16–18]. Campus green spaces play a vital role in achieving carbon neutrality and net-zero emissions due to their significant potential for carbon offset[2,19–21]. In Southeast Asia, where high-density, island-based populations face land constraints, urban green spaces emerged as a crucial focus for achieving net-zero carbon emissions despite spatial limitations[22,23]. In the current environment, especially for urban areas, establishing green spaces to support achieving net-zero carbon emissions in Southeast Asian countries presents significant challenges. The existing green spaces, especially campus green spaces in urban areas, serve as a potential solution. Campus green spaces have extensive and well-maintained green coverage, making them valuable components for achieving net-zero carbon emissions. Moreover, campus green spaces can serve as essential green infrastructure, providing not only carbon storage, but also enhancing biodiversity and reducing air-pollution[24,25]. Research has demonstrated that campus environments are effective living labs for sustainability research[26]. Campus green spaces have explicit boundaries. They are governed by well-defined management protocols and maintain extensive vegetated areas[27,28]. Together, these features make them ideal sites for high-resolution carbon monitoring and validation. Additionally, research on campus green spaces can inform urban planning in terms of ecosystem services[29]. Based on the carbon storage potential and environmental co-benefits, this research targets campus green spaces.

Despite campus green spaces' relatively small geographic scope, research shows that two of the most common tools for conducting the campus carbon storage investigation are tree inventories and remote sensing[15–17,19]. Campus tree inventories typically estimate carbon storage and carbon sequestration by measuring DBH, height, and species[28,30,31]. The majority of the campus green space carbon storage and sequestration relies on the campus tree inventories[27]. As for the remote sensing approach, UAV is one of the most common platforms due to the relatively small geographic scope of campus green space[13,25]. Notably, research has shown that remote sensing approach can potentially be a more cost-effective approach[16]. Despite remote sensing's advantages and its long-standing utilization in forest carbon storage research, only a few cases have adopted a remote sensing approach to investigate the carbon storage and sequestration issue in campus green spaces[27,32–34].

Different remote sensing approaches have distinct advantages in estimating carbon sequestration and storage[35–40]. In remote sensing, multispectral imagery was one of the most common data sets for assessing plants' growing status and Net Primary Productivity (NPP). NPP represents the net accumulation of organic matter through carbon fixation via photosynthesis per unit area and time, which could be regarded as the carbon sequestration of the vegetation[41,42]. NPP can be regarded as a proxy for carbon sequestration potential, which is one of the most essential indices for achieving carbon neutrality and addressing climate change challenges. The Carnegie-Ames-Stanford Approach (CASA) was one of the approaches that used multispectral imagery to estimate the NPP of the vegetation. CASA was a biophysical-based model that estimated the NPP of trees and grass using the Vegetation Index (VI) derived from multispectral imagery, including Normalized Difference Vegetation Index (NDVI) and Simple Ratio (SR) alongside solar radiation (SOL), temperature, and water stress factor (WSF)[43–46]. The VI, such as NDVI and SR, were adopted to estimate the Fraction of Photosynthetically Active Radiation (FPAR) based on the linear relationship. With the FPAR and SOL, the APAR was computed. The temperature was adopted to calculate the $T_{\varepsilon 1}$ and $T_{\varepsilon 2}$, representing the constraint of temperature variation to vegetation[43–45]. WSF was calculated using Potential Evapotranspiration (PET) and Actual Evapotranspiration (AET) to represent the constraint to vegetation from environmental water scarcity. The calculation of PET and AET required unique meteorology parameters, causing the data spatial distribution to be uneven. This made the WSF commonly regarded as an uncertain factor[42,47]. Finally, the light use efficiency (ε) was calculated by the $T_{\varepsilon 1}$, $T_{\varepsilon 2}$, WSF, and ε_{max}. The APAR and ε were then estimated for the NPP. Also, several studies demonstrated CASA's reliability and robustness[47–49].

To estimate the NPP of campus green space, the approach we proposed leveraged the benefits of UAV and satellite multispectral images. UAV multispectral images provided a canopy-level of spatial resolution with high temporal resolution[50–52], making UAV VIs a perfectly tailored tool for computing the FPAR that CASA needed. Satellite images provided not only commonly seen Red, Green, and Blue bands but also near-infrared (NIR) and shortwave infrared (SWIR) data[53–55], particularly the SWIR. SWIR represented the environmental water content[56]. SWIR was highly related to the content within the soil and vegetation and was adopted to calculate the WSF[42,57]. The correctness of NPP estimation was highly related to correctly identifying the area of campus green space. Thus, we adopted a machine learning-based image classification algorithm, Random Forest (RF) classification, to identify and extract campus green spaces. Finally, we proposed a CASA^{+}UAV with a multi-source approach, leveraging the advantage of UAV and satellite multispectral images to estimate the NPP of campus green spaces. The main aim of this research was to propose an approach that integrated (1) RF classification, (2) CASA, (3) UAV multispectral images, and (4) Satellite images to offer a practical and accurate approach to

Class	Water	Built-Up	Barren	Forest	Herbaceous	Total	User Accuracy	Kappa
Water	997.887	15.841	0.000	5.018	0.016	1018.762	0.980	
Built-Up	22.583	18,063.869	1080.040	27.568	1.092	19,195.152	0.941	
Barren	0.000	526.684	7395.048	18.707	69.432	8009.871	0.923	
Forest	0.008	4.221	0.172	9803.434	259.885	10,067.720	0.974	
Herbaceous	0.000	7.933	5.831	127.811	1739.668	1881.242	0.925	
Total	1020.479	18,618.548	8481.091	9982.538	2070.093	40,172.748		
Producer Accuracy	0.978	0.970	0.872	0.982	0.840		0.946	
Kappa								0.919

Table 1. The confusion matrix of the RF classification result.

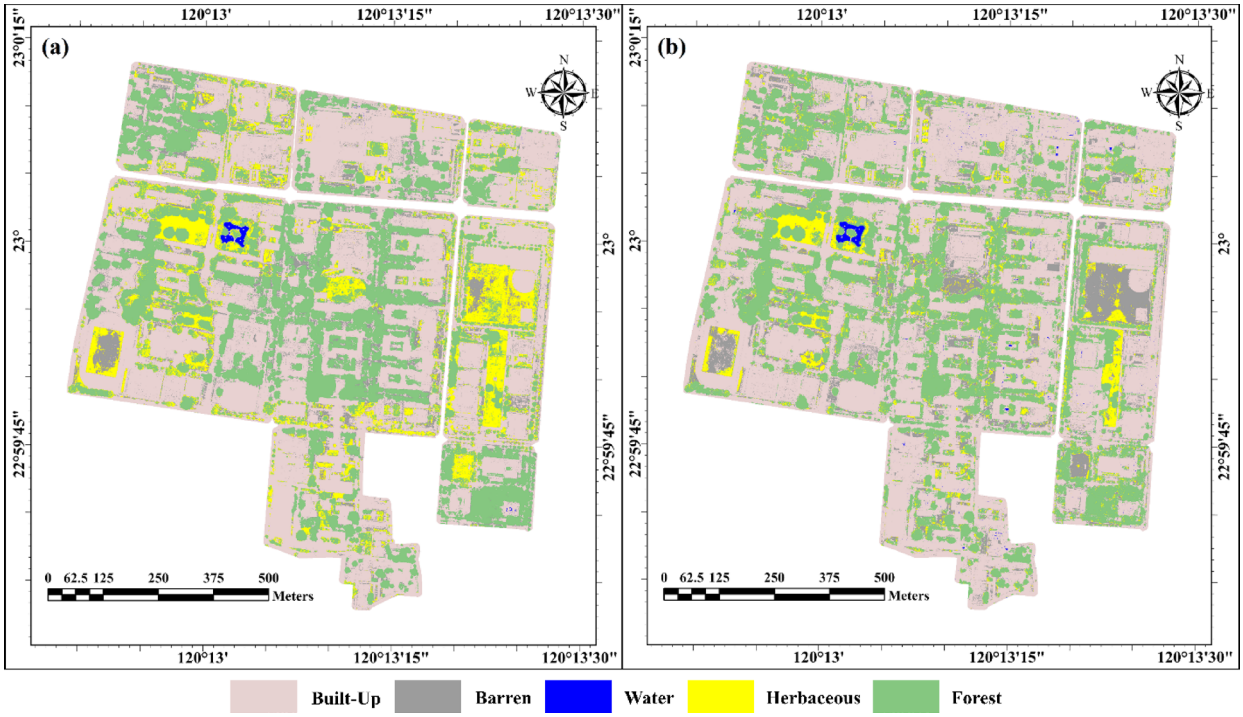

Fig. 1. The result of RF classification of NCKU in July 2023 (**a**) and May 2024 (**b**).

estimate the NPP of campus green space. To ensure our approach's effectiveness and accuracy, we compared the NPP estimated based on (1) CASA$^+$UAV with WSF calculated based on satellite images (WSF(Multi-Source)), (2) CASA$^+$UAV with the WSF driven by PET and AET (WSF(Original)), and (3) the ground-estimated NPP. The ground-estimated NPP was estimated based on the complete enumeration of experimental plots in our study site. The Diameter at Breast Height (DBH), Tree Height (TH), and species were recorded and used to estimate the NPP.

Results

RF classification and green space extraction

To properly extract the green space, VIs data were essential. First, 14 VIs were generated based on the VI calculation default setting from ArcGIS Pro 3.3. Next, all the VIs were composited with the UAV multispectral image for RF classification to extract the area of green space. To classify the UAV multispectral image, 183 training polygons were delineated by on-screen interpretation and field reference. The classification schema includes Forest, Herbaceous, Water, Built-Up, and Barren. For validation, 131 independent validation polygons were adopted for further calculation of the Confusion matrix, overall accuracy, and Kappa coefficient. Table 1 demonstrates the confusion matrix and results. The classification results' overall accuracy and Kappa coefficient were 0.946 and 0.919, respectively. According to the confusion matrix, the RF classification result is reliable for extracting the green space for further NPP estimation. Figure 1 demonstrates the RF classification results of July 2023 and May 2024.

In 2023, the areas of Forest and Herbaceous were 27.61 and 8.28 ha, respectively, while Water, Built-Up, and Barren covered 0.26, 47.03, and 5.05 ha. By 2024, Forest and Herbaceous areas decreased to 26.34 and 4.11 ha, respectively, while Water, Built-Up, and Barren measured 0.25, 48.49, and 9.02 ha. The analysis revealed notable variations in green space areas between the two observation dates, with extracted green space decreasing from 35.89 ha on July 1, 2023, to 30.45 ha on May 4, 2024.

As a typhoon-prone region, Taiwan employs proactive landscape management strategies on its campuses. The forest areas were affected by Typhoon Haikui in September 2023, which caused tree toppling. To mitigate potential hazards, the university conducted preventive tree crown pruning between the two observation periods. This management practice, combined with natural typhoon impacts, contributed to the observed reduction in forest coverage.

Herbaceous areas also exhibited notable changes, primarily driven by seasonal variations. According to MODIS data, June and July represent the peak periods of vegetation growth in Taiwan, characterized by optimal NDVI values. Compared to May, July experiences higher precipitation and temperature, which typically enhances vegetation density. This seasonal difference explains the lower herbaceous coverage observed in May 2024 compared to July 2023, reflecting the natural phenological cycle rather than a permanent change in land cover.

Model verification

To assess model accuracy, NPP estimated using ground-based parameters was compared against CASA$^+$UAV with WSF(Multi-Source) and CASA$^+$UAV with WSF(Original) for July 2023 and May 2024. For CASA$^+$UAV with WSF(Multi-Source), R^2 values were 0.79 and 0.68, surpassing the 0.75 and 0.65 for WSF(Original). The MAE was 3.28 and 6.33 $gC{\cdot}m^{-2}{\cdot}month^{-1}$ for WSF(Multi-Source) compared to 19.89 and 18.68 $gC{\cdot}m^{-2}{\cdot}month^{-1}$ for WSF(Original). MAPE values for WSF(Multi-Source) were 4.37% and 8.43%, while WSF(Original) showed 26.50% and 24.88%. RMSE for CASA$^+$UAV with WSF(Multi-Source) was 11.74 and 17.01 $gC{\cdot}m^{-2}{\cdot}month^{-1}$, and for WSF(Original) it was 23.14 and 25.39 $gC{\cdot}m^{-2}{\cdot}month^{-1}$. Likewise, %RMSE for CASA$^+$UAV with WSF(Multi-Source) was 15.63% and 22.65%, compared to 30.83% and 33.82% for WSF(Original). Figure 2 shows the model validation results and highlights the better performance of CASA$^+$UAV with WSF(Multi-Source). Figures 2(b) and (d) indicate that CASA$^+$UAV with WSF(Original) likely overestimates NPP, while CASA$^+$UAV with WSF(Multi-Source) delivers higher R^2 and less bias.

Estimations of campus green space NPP

The NPP of NCKU green spaces estimated by CASA$^+$UAV with WSF(Multi-Source) in July 2023 and May 2024 was illustrated in Fig. 3. In July 2023, the mean NPP for campus green spaces was 76.19 ± 27.58 $gC{\cdot}m^{-2}{\cdot}month^{-1}$, with values ranging from 6.85 to 164.87 $gC{\cdot}m^{-2}{\cdot}month^{-1}$. The cumulative NPP for the entire NCKU campus reached 27,349.19 $kgC{\cdot}month^{-1}$ in July 2023. In an analysis encompassing each campus in NCKU, in July 2023, Campus B (KF) had the highest mean and cumulative NPP, which were 80.77 ± 27.11 $gC{\cdot}m^{-2}{\cdot}month^{-1}$ and 7784.12 $kgC{\cdot}month^{-1}$. Followed by Campus D (CK) with 77.46 ± 27.58 $gC{\cdot}m^{-2}{\cdot}month^{-1}$ and 6736.55 $kgC{\cdot}month^{-1}$, and Campus A (LH) with 76.77 ± 27.19 $gC{\cdot}m^{-2}{\cdot}month^{-1}$ and 3116.21 $kgC{\cdot}month^{-1}$.

In May 2024, the mean NPP of the green space on campus was 81.48 ± 33.89 $gC{\cdot}m^{-2}{\cdot}month^{-1}$, with values ranging from 7.71 to 175.77 $gC{\cdot}m^{-2}{\cdot}month^{-1}$. The total campus green space cumulative NPP was 24,811.044 $kgC{\cdot}month^{-1}$. According to the analysis of eight campuses in NCKU in May 2024, Campus B had the mean and cumulative NPP 85.72 ± 35.07 $gC{\cdot}m^{-2}{\cdot}month^{-1}$ and 7467.81 $kgC{\cdot}month^{-1}$. The mean and cumulative NPP of Campus D were 81.29 ± 33.99 $gC{\cdot}m^{-2}{\cdot}month^{-1}$ and 6214.96 $kgC{\cdot}month^{-1}$. Finally, the mean and cumulative NPP of Campus A were 85.76 ± 32.24 $gC{\cdot}m^{-2}{\cdot}month^{-1}$ and 3177.27 $kgC{\cdot}month^{-1}$. The results of comparing eight campuses between 2023 and 2024 were quite similar. The only difference is that Campus A has the highest mean NPP.

The net primary productivity (NPP) of campus green spaces showed relative consistency over the study period, though multi-year data are needed to confirm stability. Despite external influences such as typhoons, anthropogenic activities, and seasonal fluctuations, the mean NPP of these green spaces remained stable, with a mean difference of only 5.29 $gC{\cdot}m^{-2}{\cdot}month^{-1}$ between 2023 and 2024. The disparity in mean NPP values across all campuses was also minimal, with differences of 10.13 and 12.35 $gC{\cdot}m^{-2}{\cdot}month^{-1}$ for 2023 and 2024, respectively. Campuses B, D, and A consistently ranked highest in NPP values. The elevated productivity observed in Campuses B and D can be attributed to several interrelated factors. Both campuses constitute the oldest portions of NCKU, established during the Japanese colonial period around 1931, and consequently support mature tree stands with well-developed canopy structures. Campus B features the iconic Banyan Park, one of the largest contiguous green spaces within NCKU boundaries, while Campus D contains extensive vegetated corridors, including Engineering Avenue and the Art Garden. These historical campuses are characterized by larger, less fragmented green cores that minimize edge effects and reduce shading interference from built structures. This spatial configuration facilitates higher per-unit-area NPP and yields greater cumulative carbon sequestration, as a productive canopy occupies a larger proportion of the total campus footprint. The presence of mature vegetation in these older campuses also suggests greater structural complexity and leaf area index, both of which positively influence photosynthetic capacity and carbon uptake.

Campus A ranked third, notably housing Taiwan's first net carbon–neutral green building, the Green Technology Magic School (MSGT), which integrates sustainable architectural design with extensive greenery. The relatively low inter-campus variance in NPP suggests that systematic vegetation management practices across NCKU effectively maintain ecosystem productivity.

These findings indicate that long-term landscape maturation, spatial continuity of green infrastructure, and consistent maintenance protocols are key determinants of carbon sequestration capacity in urban campus environments.

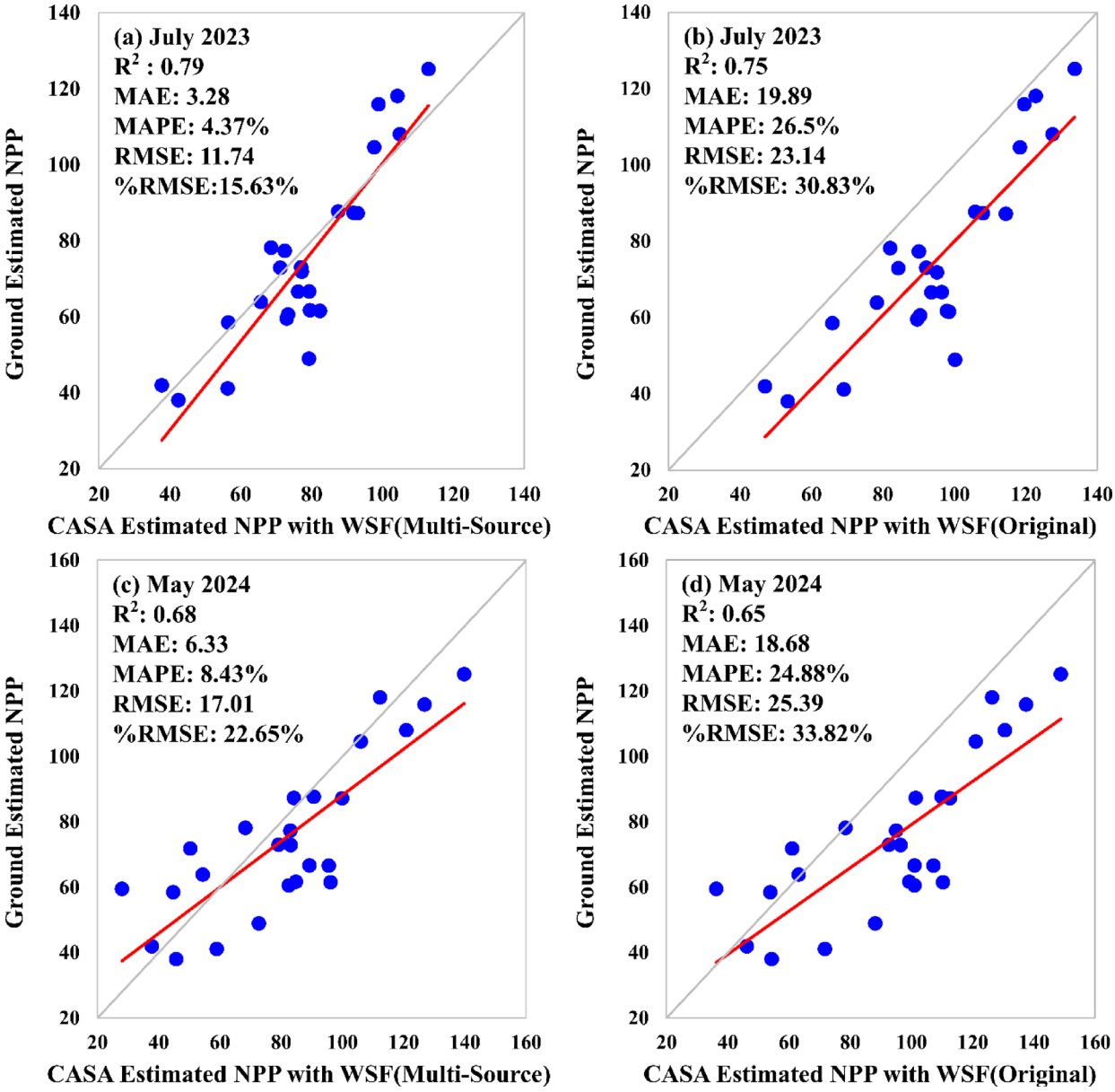

Fig. 2. The result of comparing Ground Estimated NPP and different CASA⁺UAV approaches. (**a**) and (**c**) show the comparison between Ground Estimated NPP and CASA⁺UAV with WSF(Multi-Source) estimated NPP. (**b**) and (**d**) show the comparison between Ground Estimated NPP and CASA⁺UAV with WSF(Original) estimated NPP.

From a management perspective, these results support the prioritization of preserving established green spaces and promoting landscape connectivity when planning future campus development to optimize ecosystem services.

Discussion

NPP, a proxy for carbon sequestration potential, is one of the most essential indices for achieving carbon neutrality and addressing climate change challenges. The assessment of NPP must be conducted with meticulous precision, accounting for even the most minute details. Campus green spaces, one of the most common types of urban green spaces, are valuable components that can support carbon neutrality[2,16,22]. Although widespread, fragmented urban green spaces, especially those on campuses, remain underexplored, even as their carbon-offset potential makes them pivotal to achieving carbon neutrality and net-zero strategies[16–21]. In Southeast Asia's densely populated, land-constrained cities, campus grounds offer readily available, well-maintained green spaces that can contribute to net-zero targets, particularly when creating new parks is challenging[22,23]. Beyond carbon, campus landscapes serve as essential green infrastructure, enhancing biodiversity and mitigating air pollution to deliver co-benefits for urban health and resilience[24,25]. Their explicit boundaries, defined management protocols,

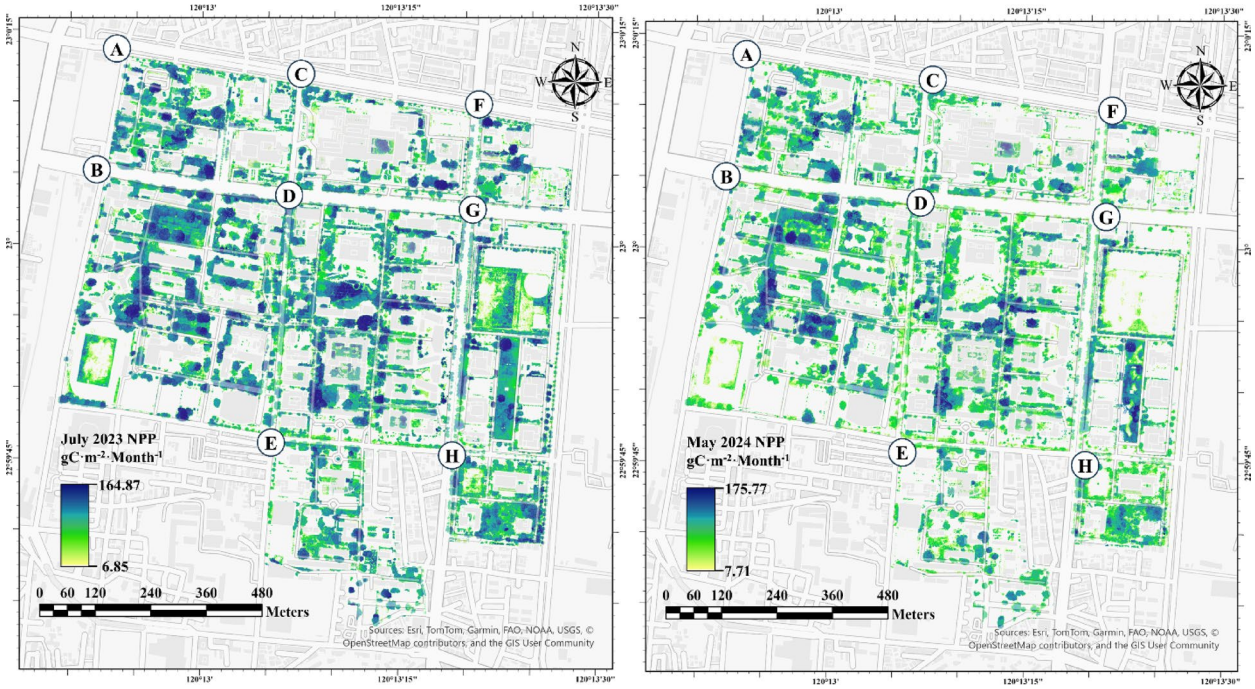

Fig. 3. The result of CASA⁺UAV with WSF(Multi-Source) of NCKU in July 2023 and May 2024.

and extensive vegetated areas enable high-resolution monitoring, ground validation, and method development with UAV and satellite observations[26–28]. Evidence generated on campus scales has the potential to be applied to city practice by quantifying ecosystem services and offering policy-relevant demonstrations for carbon–neutral and sustainable urban planning[29].

To address the special geographical scale of campus green space, we proposed a high-resolution approach that integrates a machine learning classification algorithm and multi-source remote sensing data to precisely estimate the NPP of campus green space. Classification provides the essential vegetation information for NPP estimation in the CASA model. RF classification is robust and highly accessible without coding a machine learning-based algorithm. Typically, the overall accuracy of classification results ranges from 80 to 90%[47,48]. With an overall accuracy of 94.6% and a Kappa coefficient of 0.919, the RF classification demonstrated exceptional accuracy in distinguishing between vegetation and non-vegetation. Such precision is critical for the accurate extraction of green space and the reliable estimation of NPP.

With vegetation accurately classified, we refined the CASA model for campus green space NPP estimation through two key methodological improvements. This study advances campus green space applications of CASA with two methodological refinements. (1) Enhanced spatial resolution via UAV integration. Standard CASA implementations rely on 20–30 m satellite inputs, which are often too coarse for campuses where vegetation patches can be smaller than a pixel. Incorporating UAV multispectral imagery provides centimeter-level inputs for FPAR, improving representation of fragmented green spaces and reducing mixed-pixel effects. (2) Reduced WSF uncertainty via satellite-based moisture retrieval. Conventional WSF estimation requires calculating actual evapotranspiration (AET) and potential evapotranspiration (PET) from ground meteorological station data[43–45], which can be unevenly distributed or insufficient in spatial coverage. This approach necessitates spatial interpolation that may introduce uncertainties in heterogeneous urban settings[42,47]. We instead derive WSF directly from Sentinel 2 SWIR/NIR reflectance at 20 m resolution, providing spatially distributed moisture information without extensive interpolation. Together, these refinements address key limitations of spatial resolution and WSF uncertainty noted in prior campus green space NPP studies, enhancing the applicability of CASA to fragmented urban green spaces.

To evaluate the performance of our approach, we validated the CASA⁺UAV with WSF(Multi-Source) method against ground-estimated NPP and compared it with the conventional CASA⁺UAV with WSF(Original) approach. The validation results demonstrated satisfactory performance, with coefficient of determination values of 0.79 and 0.68 for July 2023 and May 2024, respectively, and relatively low error metrics. These results are comparable to those reported in previous urban NPP studies[58–60], supporting the reliability of our integrated approach.

For the NCKU campus, the total number of sampling plots used for validation is twenty-five, with each plot measuring 30 m by 30 m. This relatively limited number of plots may constrain the spatial representativeness of the validation results. To further assess the robustness and transferability of our approach, we applied the same CASA⁺UAV with WSF(Multi-Source) method to two additional sites: Chung-Wen Elementary School and Sing-Chia Elementary School in Chiayi City, commissioned by the Chiayi City Government in 2023. Independent validation was conducted using 20 plots at Chung-Wen and 36 plots at Sing-Chia. The validation results

demonstrated comparable performance, with R^2 values of 0.72 and 0.70, and RMSEs of 27.33 $gC{\cdot}m^{-2}{\cdot}month^{-1}$ and 35.16 $gC{\cdot}m^{-2}{\cdot}month^{-1}$, respectively. Results from two other schools support the robustness and transferability of the proposed method, thereby alleviating concerns regarding the limited number of validation plots at the primary study site.

Beyond validation accuracy, we assessed whether our NPP estimates align with published values from comparable urban environments. In our study, campus green space NPP ranged from 76.19 to 81.48 $gC{\cdot}m^{-2}{\cdot}month^{-1}$ between July 2023 and May 2024. These values can be compared with observations from other urban areas using CASA with similar latitudes or coastal locations in subtropical China. The first comparable case is from Guangzhou, where the average NPP of urban green space was 83.12 $gC{\cdot}m^{-2}{\cdot}month^{-1}$[61]. A second case from the Pearl River Delta region—encompassing Guangzhou, Foshan, Dongguan, Zhongshan, Shenzhen, Zhuhai, Huizhou, Zhaoqing, and Jiangmen—reported an average summer urban green space NPP of 95.71 $gC{\cdot}m^{-2}{\cdot}month^{-1}$[62]. Finally, in Wuhan during 2017–2020, monthly NPP ranged from 30 to 65 $gC{\cdot}m^{-2}{\cdot}month^{-1}$ in May and 50 to 80 $gC{\cdot}m^{-2}{\cdot}month^{-1}$ in July[47]. The comparisons suggest that our estimated results fall within the range observed from other urban green space in similar climatic zones, though variations exist due to differences in geographical location, vegetation composition, and seasonal timing. Building on this cross-city context, temporal analysis between July 2023 and May 2024 indicates that, despite seasonal fluctuations and post-Typhoon Haikui crown pruning that reduced total green-space area, mean NPP per unit area remained relatively consistent between the two observation periods, suggesting the potential capacity of managed campus green spaces to maintain productivity under disturbance. However, longer-term monitoring is needed to confirm this pattern across multiple years and varying climatic conditions.

Despite the promising outcomes, the study has several technical limitations. First, understory detectability is constrained by canopy occlusion: vegetation growth and 3D structure are tightly coupled. Although our workflow can produce high-accuracy surface models, passive optical sensors lack canopy penetration, limiting the detection of sub-canopy and shaded vegetation beneath tall trees. Second, sensor and platform constraints remain: integrated RGB–NIR–SWIR payloads are uncommon; SWIR sensors are heavier and often require custom mounts, which raises payload, safety, and signal-stability concerns (e.g., vibration, power, and thermal management). Third, the use of non-metric cameras can introduce uncertainty in interior orientation parameters and lens distortion, which may propagate into georegistration and reflectance retrieval. Finally, despite good performance in this case study, confirming robustness will require multi-year monitoring and cross-site validation to quantify interannual variability and disturbance responses. Notwithstanding these limitations, we anticipate further performance gains if UAV payloads can include co-boresighted RGB, NIR, and SWIR sensors. Nevertheless, within current constraints, our results indicate that the approach provides accurate and precise estimates for campus green spaces.

This research contributes to the evolving body of knowledge on urban and campus carbon management by offering an operationally efficient, adaptable, and scalable approach to assessing NPP as a proxy for carbon sequestration potential in our case study. Based on our results, the proposed approach can capture the NPP provided by campus green spaces with a higher R^2 and lower RMSE compared to traditional CASA. Additionally, this research highlights the role of campus green spaces as potentially effective carbon sinks within urban areas, which might facilitate and contribute to achieving carbon neutrality at the city or urban level. In the face of climate change and the emerging carbon trading market, our research provides valuable insights and tools for policymakers and urban planners seeking to leverage green infrastructure as part of climate action strategies.

With global temperatures surpassing the 1.5 °C threshold, as reported by Copernicus Climate, the need to urgently strive for carbon neutrality becomes even more pronounced. This is a pivotal goal in our battle against climate change, crucial for stabilizing our climate and preventing further detrimental effects. Our research contributes to this vital effort by providing an accurate, precise, low-cost, and efficient tool to assess the NPP of campus green spaces. Our results suggest that, when adequately managed, campus green spaces can function as effective urban carbon sinks; however, broader and longer-term observations are required to confirm this across sites and seasons. These findings provide evidence to guide city-level carbon neutrality and urban green-infrastructure planning in densely populated environments where natural land resources are limited. Moreover, our research lends support to urban greening initiatives by offering innovative tools that integrate UAV multispectral imagery, Random Forest (RF) classification, and Sentinel 2 satellite data. This practical and scalable approach provides a robust solution for urban planners and policymakers to evaluate and enhance carbon sequestration in urban areas, thereby contributing to the broader fight against climate change. In conclusion, this research advances urban carbon sequestration assessment by integrating UAV imagery, the CASA model, and multi-source remote sensing data. Our approach addresses key challenges in evaluating urban green spaces, particularly in densely populated areas with limited resources. The relatively consistent NPP observed across two dates suggests potential stability, though multi-year monitoring is needed before confirming long-term stability. This study offers a cost-effective and reliable methodology for urban planners and policymakers, providing valuable insights for leveraging green infrastructure in climate action and supporting global climate mitigation efforts.

Methods

Study site

The study site of this research was National Cheng Kung University (NCKU), situated in Tainan City, southern Taiwan. NCKU was adjacent to the Tainan Railway Station in the city's central area. The NCKU campus in central Tainan City was one of the largest in Tainan, encompassing an area of 76.3 hectares, which accounted for 17.6% of all university campus areas within the city. Notably, over 41% of the campus was covered with expansive green spaces, the highest proportion among all universities in Tainan City. Tainan City was the most ancient city

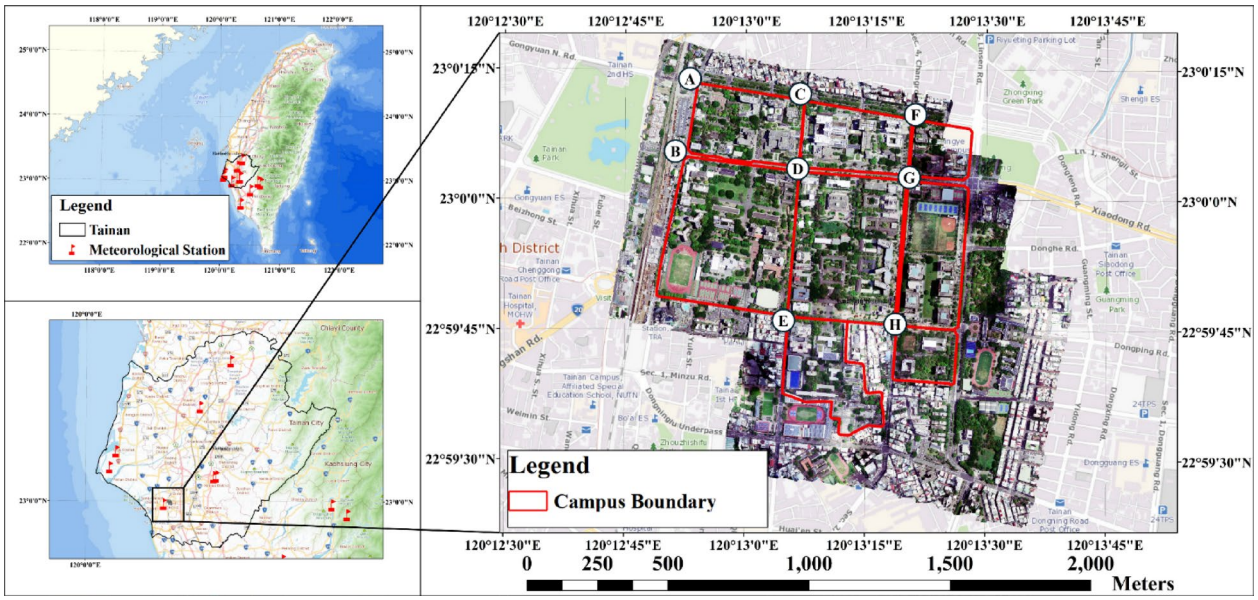

Fig. 4. The location of the NCKU campus and meteorological station. (**A**): Li-Hsing (LH) Campus; (**B**): Kuang-Fu (KF) Campus; (**C**): Cheng-Hsin (CH) Campus; (**D**): Cheng-Kung (CK) Campus; (**E**): Sheng-Li (SL) Campus; (**F**): Ching-Yeh (CY) Campus; (**G**): Tzu-Chiang (TC) Campus; (**H**): Tung-Ning (TN) Campus.

in Taiwan. This led to a densely populated and crowded urban area with limited green spaces. Consequently, NCKU became a crucial urban green space. The study site is illustrated in Fig. 4.

UAV multispectral imagery

In the collection of primary green space data extracted from multispectral images, the A3 Fun II Drone A610, a six-rotor UAV, was used. The sensor used in this research was the MicaSense RedEdge-P. This sensor included multispectral and panchromatic sensors. Both sensors had an identical pixel size, which was 3.45 µm. The radiometric resolution was 12-bit. The multispectral sensors provided blue (475 nm), green (560 nm), red (668 nm), red-edge (717 nm), and NIR (842 nm). The UAV aerial photography was conducted on July 1st, 2023, and May 4th, 2024. The bundle block adjustment was conducted to generate an aerial orthophotograph. In this research, bundle block adjustment was conducted by Pix4D. The Topcon Hiper-VR GNSS rover acquired the Ground Control Points (GCPs) for the orthophotograph. Sufficient overlap was essential to ensure the result of the bundle block adjustment. The across-track and along-track overlap of this research was 80%. The flight height of this research was 150 m. The final orthophoto had a ground spatial resolution of 10 cm.

Sentinel 2 imagery

We used the Sentinel 2 L2A SWIR band and NIR band to calculate the WSF required by the CASA model. The spatial resolution of the SWIR and NIR bands was 20 m and 10 m, respectively. Studies leveraged multispectral imagery for WSF estimation[42,57,60,63], highlighting its advantage over traditional methods that relied on ground meteorological data and spatial interpolation. Compared to the spatial distribution of the meteorological stations, remote sensing data provided at least one observation every 20 m. Remote sensing data afforded a comprehensive observation of the study area, helping to reduce uncertainties associated with sparse station coverage and interpolation. To align the Sentinel 2 imagery with the UAV orthophotograph, 4-parameter transformation image co-registration was adopted.

Meteorological data

The data on temperature and SOL required for CASA originated from observations made by a total of 11 ground meteorological stations in southern Taiwan, managed by the Central Weather Administration and the Taiwan Agricultural Research Institute. The temperature and SOL obtained from these ground meteorological stations were used to compute the $T_{\varepsilon 1}$, $T_{\varepsilon 2}$, PET, AET, and SOL.

Development of CASA$^+$UAV with a multi-source data approach

The data used in this study comprised four primary sources: (1) drone multispectral imagery, (2) Sentinel 2 imagery, (3) ground meteorological station data, and (4) campus tree survey data. Random forest classification and UAV multispectral images were initially used to extract the green space. The NIR and RED bands of green space were used to calculate the VIs and FPAR. Subsequently, the SWIR and NIR bands from Sentinel 2 were adopted to compute the WSF(Multi-Source). The ground meteorological station data were applied in the calculations of $T_{\varepsilon 1}$, $T_{\varepsilon 2}$, PET, AET, and the acquisition of SOL. PET and AET were used to calculate the WSF(Original). CASA estimated two versions of NPP. In the first version, NPP(Multi-Source), the WSF was based on the Sentinel 2 imagery. For comparison, in the second version, NPP(Original), the WSF was based on

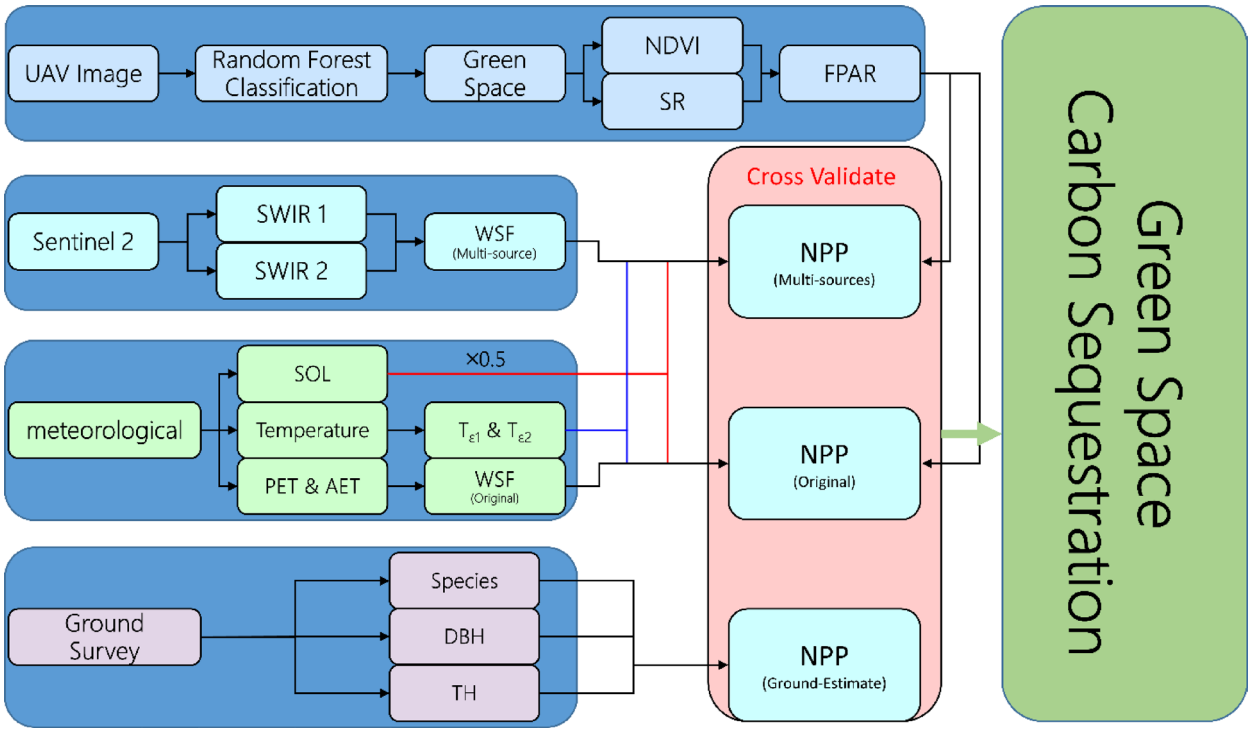

Fig. 5. The Flowchart of This Research.

the PET and AET. Finally, the two NPP estimates by CASA were cross-validated with the ground-estimated NPP based on the tree survey data. The research procedure was demonstrated in Fig. 5.

Random forest classification and green space extraction

UAV multispectral image provided a centimeter-level spatial resolution. We took advantage of the highly detailed image and the robustness of the Machine Learning-based Algorithm, the RF, to classify our study site's land use/land cover. Studies demonstrated that the RF classification properly detected the vegetation with the UAV multispectral image[64–66]. The Random Forest (RF) algorithm was comprehensively supported across both commercial and open-source remote sensing software (i.e., Sentinel Application Platform, SNAP) platforms, offering researchers and practitioners flexible implementation options for advanced geospatial analysis. ArcGIS Pro 3.3 was employed to conduct the RF classification.

To properly train and validate the RF classification, training and validation polygons were digitized based on visual interpretation and field verification. For training, 183 polygons were digitized, covering a total area of 79,383.48 m^2. For validation, 131 polygons were digitized, covering 40,012.85 m^2. Spatial overlap analysis was conducted to ensure that training and validation polygons were mutually exclusive. Five land cover classes were defined: Built-Up, Barren, Water, Herbaceous, and Forest.

Classification accuracy was assessed using a confusion matrix approach, from which Overall Accuracy (OA) and the Kappa Coefficient were derived[67–69]. Since this research adopted five classes, the Confusion Matrix is a five-by-five matrix, which is shown as follows:

$$\text{Confusion Matrix} = \begin{bmatrix} C_{11} & C_{12} & \cdots & C_{15} \\ C_{21} & C_{22} & \cdots & C_{25} \\ \vdots & \vdots & \ddots & \vdots \\ C_{51} & C_{52} & \cdots & C_{55} \end{bmatrix} \quad (1)$$

Following equation demonstrated the calculation for the OA and Kappa[67,68]:

$$\begin{aligned} \mathrm{OA} &= \frac{\sum_{i=1}^{5} C_{ii}}{\sum_{i=1}^{5}\sum_{j=1}^{5} C_{ij}} \\ \mathrm{Kappa} &= \frac{P_o - P_e}{1 - P_e} \\ P_o &= \mathrm{OA}; P_e = \frac{\sum_{i=1}^{5}(r_i \times c_i)}{N^2}; \\ r_i &= \sum_{i=1}^{5} C_{ij}; c_i = \sum_{i=1}^{5} C_{ji}; N = \sum_{i=1}^{5}\sum_{i=1}^{5} C_{ij} \end{aligned} \tag{2}$$

C_{ij} represents areas (square meters) whose true class is i but predicted class is j. The diagonal elements C_{11} to C_{55} are the correctly classified samples for each class. P_o, the Observed Agreement represents the empirical proportion of concordant classifications in the data[68,69]. It is calculated as the sum of the diagonal elements of the confusion matrix divided by the total number of observations[69]. P_e is the Expected Agreement, representing the theoretical proportion of agreement that would occur by chance alone, assuming statistical independence between the two classifications while preserving their marginal distributions[68,69].

Development of the CASA model

CASA and detailed parameters for the multi-source data approach were provided below. The CASA estimated the NPP of vegetation by the ε and APAR (MJ m^{-2}), first proposed by [43] based on satellite multispectral imagery. The CASA model was driven by the NDVI, temperature, and WSF. NPP was calculated by the following equation[46,70]:

$$\mathrm{NPP} = \mathrm{APAR} \times \varepsilon \tag{3}$$

APAR is calculated as the following equation:

$$\mathrm{APAR} = \mathrm{SOL} \times \mathrm{FPAR} \times 0.5 \tag{4}$$

SOL was the monthly total solar radiation (MJ m^{-2}). 0.5 was the constant that represents the proportion of the photosynthetically available radiation, range from 0.38 to 0.71 μm[42–45]. FPAR stands for a fraction of the photosynthetically active radiation absorbed by the vegetation canopy, which is calculated based on NDVI and SR through the following equation[58,59,71,72]. The $\mathrm{FPAR}_{\mathrm{max}}$ and $\mathrm{FPAR}_{\mathrm{min}}$ were constant, and the values were 0.950 and 0.001, respectively.

$$\begin{aligned} \mathrm{FPAR_{SR}} &= \frac{(\mathrm{SR_n} - \mathrm{SR_{min}}) \times (\mathrm{FPAR_{max}} - \mathrm{FPAR_{min}})}{\mathrm{SR_{max}} - \mathrm{SR_{min}}} + \mathrm{FPAR_{MIN}}; \\ \mathrm{FPAR}_{NDVI} &= \frac{(\mathrm{NDVI_n} - \mathrm{NDVI_{min}}) \times (\mathrm{FPAR_{max}} - \mathrm{FPAR_{min}})}{\mathrm{NDVI_{max}} - \mathrm{NDVI_{min}}} + \mathrm{FPAR_{MIN}}; \\ \mathrm{FPAR} &= \alpha \mathrm{FPAR}_{SR} + (1-\alpha)\,\mathrm{FPAR}_{NDVI};\ \alpha = 0.5 \\ \mathrm{NDVI} &= \frac{\rho NIR - \rho RED}{\rho NIR + \rho RED} \\ SR &= \frac{1 + NDVI}{1 - NDVI} \end{aligned} \tag{5}$$

The calculation of the ε was based on the temperature, WSF, and $\varepsilon_{\mathrm{max}}$ through the following equation[43,44]:

$$\varepsilon = \mathrm{WSF} \times \mathrm{T}_{\varepsilon 1} \times \mathrm{T}_{\varepsilon 2} \times \varepsilon_{\mathrm{max}} \tag{6}$$

For the WSF, in this research we used two different approaches to calculate two versions of the WSF. For the first version, WSF(Multi-Source), was calculated according to Sentinel 2 SWIR and NIR based on the equation shown as follows[49,57,60,61,72,73]. The ρNIR and ρSWIR are the reflectance of the NIR and SWIR. The WSF(Multi-Source) was calculated as following equation.

$$\mathrm{WSF(multi-sources)} = \frac{1 + \left(\frac{\rho_{\mathrm{NIR}} - \rho_{\mathrm{SWIR}}}{\rho_{\mathrm{NIR}} + \rho_{\mathrm{SWIR}}}\right)}{1 + \left(\frac{\rho_{\mathrm{NIR}} - \rho_{\mathrm{SWIR}}}{\rho_{\mathrm{NIR}} + \rho_{\mathrm{SWIR}}}\right)_{\mathrm{max}}} \tag{7}$$

In parallel, we implemented a benchmark WSF(original) following the conventional CASA formulation of [43], in which the water-stress factor is derived from AET and PET. Estimating AET and PET requires ground-based meteorological observations; thus, station records were spatially interpolated to produce wall-to-wall fields over the study area[47]. However, the limited number and uneven spatial distribution of stations, together with the pronounced spatial heterogeneity of urban landscapes, can introduce interpolation uncertainty[42,47]. Accordingly, NPP derived with WSF(original) is used solely as a baseline for comparison with NPP based on the Sentinel 2-based WSF(multi-source).

Finally, $T_{\varepsilon 1}$ and $T_{\varepsilon 2}$ stand for the temperature parameters that affect photosynthesis. $T_{\varepsilon 1}$ and $T_{\varepsilon 2}$ are calculated through Eqs. (8) and (9) [42,46]. T and T_{opt} stand for the mean monthly temperature of the multispectral image and the mean monthly temperature with the highest NDVI index. Finally, ε_{max} was based on the tree species.

$$T_{\varepsilon 1} = 0.8 + 0.02 \times T_{opt} - 0.0005 \times (T_{opt})^2 \tag{8}$$

$$T_{\varepsilon 2} = \frac{1.1814}{\left[1 + e^{0.2\times(T_{opt}-10-T)}\right] \times \left[1 + e^{0.3\times(-T_{opt}-10+T)}\right]} \tag{9}$$

Ground validation

The ground-estimated NPP was measured to validate the result of CASA$^+$UAV with a multi-source data approach. Twenty-five sampling plots with a size of 30 × 30 m were established. The tree height (H) and diameter at breast height (DBH) were measured for subsequent estimation of ground-estimated NPP. The following equation calculates the ground-measured NPP according to[74].

$$\mathrm{NPP} = \mathrm{RGR} \times \mathrm{Biomass} \tag{10}$$

The RGR proposed by[74] was adopted and converted to a monthly rate (g g^{-1} $month^{-1}$). The allometric equation for the estimation of tropical forest aboveground biomass proposed by[75] was adopted in our research. The equation was shown as follows.

$$\mathrm{Biomass} = 0.0673 \times \left(\rho \times \mathrm{DBH}^2 \times \mathrm{H}\right)^{0.976} \times (1 + \mathrm{R}) \times \mathrm{BEF} \times \mathrm{CF} \tag{11}$$

The ρ in the equation was the wood density. DBH was the diameter at breast height. H was the tree height. R was the ratio of the aboveground biomass to the belowground biomass. BEF was the Biomass Expansion Factor. CF was the carbon fraction. The ρ, BEF, and CF were acquired from the Database for Carbon Stocks Estimation Variables of Tree Species Used in Soil and Water Conservation (https://tech.ardswc.gov.tw/Education/PlantCarbon) and National Greenhouse Gas Inventories-Land Use, Land Cover, and Forestry (https://service.cca.gov.tw/File/Get/cca/zh-tw/zfgeB77vAQc4SHK).

Data availability

The UAV, Sentinel 2 satellite imageries, and meteorological data were downloaded from the following public resources: UAV Image: https://doi.org/10.5281/zenodo.15016312. Sentinel 2 Satellite Imagery: https://browser.dataspace.copernicus.eu/. Meteorological Data: https://codis.cwa.gov.tw/StationData

Received: 28 August 2025; Accepted: 10 November 2025
Published online: 24 December 2025

References

1. Sowińska-Świerkosz, B. & García, J. What are Nature-based solutions (NBS)? Setting core ideas for concept clarification. *Nat. Base Solu.* **2**, 100009. https://doi.org/10.1016/j.nbsj.2022.100009 (2022).
2. Pan, H. et al. Contribution of prioritized urban nature-based solutions allocation to carbon neutrality. *Nat. Clim. Chang.* **13**, 862–870. https://doi.org/10.1038/s41558-023-01737-x (2023).
3. Food and Agriculture Organization of the United Nations. *The State of the World's Forests 2018: Forest Pathways to Sustainable Development*. (FAO, 2018).
4. Nandy, S., Srinet, R. & Padalia, H. Mapping Forest Height and Aboveground Biomass by Integrating ICESat-2, Sentinel-1 and Sentinel-2 Data Using Random Forest Algorithm in Northwest Himalayan Foothills of India. *Geophys. Res. Lett.* **48**, e2021GL093799 (2021). https://doi.org/10.1029/2021GL093799
5. Silva, C. A. et al. Fusing simulated GEDI, ICESat-2 and NISAR data for regional aboveground biomass mapping. *Remote Sens. Environ.* **253**, 112234. https://doi.org/10.1016/j.rse.2020.112234 (2021).
6. Zhang, C., Li, H., Wang, X., Liu, P. & Zhan, S. Forest carbon storage in China from 2003 to 2021: Estimation based on the volume-derived carbon storage model with scale-compatible and tree species-merged. *For. Ecol. Manage.* **578**, 122483. https://doi.org/10.1016/j.foreco.2024.122483 (2025).
7. Steenberg, J. W. N. et al. A national assessment of urban forest carbon storage and sequestration in Canada. *Carbon Balance Manag.* **18**, 11. https://doi.org/10.1186/s13021-023-00230-4 (2023).
8. Iowa State University. *UI Trees*. https://maps.facilities.uiowa.edu/trees/ (2022).
9. Price, B. et al. Predicting biomass dynamics at the national extent from digital aerial photogrammetry. *Int. J. Appl. Earth Obs. Geoinf.* **90**, 102116. https://doi.org/10.1016/j.jag.2020.102116 (2020).
10. Pötzschner, F. et al. Ecoregion-wide, multi-sensor biomass mapping highlights a major underestimation of dry forests carbon stocks. *Remote Sens. Environ.* **269**, 112849. https://doi.org/10.1016/j.rse.2021.112849 (2022).
11. Chan, E. P. Y., Fung, T. & Wong, F. K. K. Estimating above-ground biomass of subtropical forest using airborne LiDAR in Hong Kong. *Sci. Rep.* **11**, 1751. https://doi.org/10.1038/s41598-021-81267-8 (2021).
12. Pascual, A., Godinho, S. & Guerra-Hernández, J. Integrated LiDAR-supported valuation of biomass and litter in forest ecosystems: A showcase in Spain. *Sci. Total Environ.* **897**, 165364. https://doi.org/10.1016/j.scitotenv.2023.165364 (2023).
13. Schick, M., Griffin, R., Cherrington, E. & Sever, T. Utilizing LiDAR to quantify aboveground tree biomass within an urban university. *Urban For. Urban Green.* **89**, 128098. https://doi.org/10.1016/j.ufug.2023.128098 (2023).
14. Qin, H., Zhou, W., Qian, Y., Zhang, H. & Yao, Y. Estimating aboveground carbon stocks of urban trees by synergizing ICESat-2 LiDAR with GF-2 data. *Urban For. Urban Green.* **76**, 127728. https://doi.org/10.1016/j.ufug.2022.127728 (2022).
15. Cornell University Campus Planning Office. *Campus Tree Inventory,* Cornell University, 2019. https://cugir.library.cornell.edu/catalog/cugir-009100 (2019).
16. Qin, S. et al. Forest emissions reduction assessment using airborne LiDAR for biomass estimation. *Resour. Conserv. Recycl.* **181**, 106224. https://doi.org/10.1016/j.resconrec.2022.106224 (2022).

17. Mngadi, M., Odindi, J. & Mutanga, O. The Utility of Sentinel-2 Spectral Data in Quantifying Above-Ground Carbon Stock in an Urban Reforested Landscape. *Remote Sens.* **13**, 4281 (2021).
18. Sun, Y., Xie, S. & Zhao, S. Valuing urban green spaces in mitigating climate change: a city-wide estimate of aboveground carbon stored in urban green spaces of China's Capital. *Glob. Chang. Biol.* **25**, 1717–1732 (2019).
19. Choudhury, M. A. M. et al. Urban Tree Species Identification and Carbon Stock Mapping for Urban Green Planning and Management. *Forests* **11**, 1226. https://doi.org/10.3390/f11111226 (2020).
20. Gülçin, D. & van den Bosch, C. C. K. Assessment of Above-Ground Carbon Storage by Urban Trees Using LiDAR Data: The Case of a University Campus. *Forests* **12**, 62. https://doi.org/10.3390/f12010062 (2021).
21. Wang, Y., Chang, Q. & Li, X. Promoting sustainable carbon sequestration of plants in urban greenspace by planting design: A case study in parks of Beijing. *Urban For. Urban Green.* **64**, 127291. https://doi.org/10.1016/j.ufug.2021.127291 (2021).
22. Huo, Z. M. et al. Estimating the contribution of community landscape construction to urban carbon neutrality: methodology and database construction. *Environ. Res. Lett.* **18**, 104035. https://doi.org/10.1088/1748-9326/acfb24 (2023).
23. Fan, Y. X. & Wei, F. Contributions of Natural Carbon Sink Capacity and Carbon Neutrality in the Context of Net-Zero Carbon Cities: A Case Study of Hangzhou. *Sustainability* **14**, 2680. https://doi.org/10.3390/su14052680 (2022).
24. Pugh, T. A. M., MacKenzie, A. R., Whyatt, J. D. & Hewitt, C. N. Effectiveness of green infrastructure for improvement of air quality in urban street canyons. *Environ. Sci. Technol.* **46**, 7692–7699 (2012).
25. van den Bosch, M. & Nieuwenhuijsen, M. No time to lose–Green the cities now. *Environ. Int.* **99**, 343–350. https://doi.org/10.1016/j.envint.2016.12.024 (2017).
26. Stuckrath, C., Rosales-Carreón, J. & Worrell, E. Conceptualisation of campus living labs for the sustainability transition: an integrative literature review. *Environ. Dev.* **54**, 101143. https://doi.org/10.1016/j.envdev.2025.101143 (2025).
27. Lee, S. et al. Tree mapping and carbon inventory on a university campus in South Korea: Case study and global review. *Ecosphere* **16**, e70118. https://doi.org/10.1002/ecs2.70118 (2025).
28. Cruz, J. R., Giordano, A. & Waliczek, T. M. Developing a university campus tree inventory and determining the value of the campus canopy through student service learning. *HortTechnology* **35**, 687–698 (2025). https://doi.org/10.21273/HORTTECH05713-25
29. Yang, Q. et al. The influence of vegetation characteristics on individual tree segmentation methods with airborne LiDAR data. *Remote Sens.* **11**, 2880 (2019).
30. University of Illinois Chicago. *Tree Inventory*. https://arborscope.com/mapDisplay.cfm?id=06CFC4C6 (2022).
31. Graham, C. et al. *SOMA District Tree Inventory Report. Community Geography Project 12.* (Portland State University, 2015). http://archives.pdx.edu/ds/psu/20536
32. Duncanson, L. et al. Aboveground biomass density models for NASA's Global Ecosystem Dynamics Investigation (GEDI) lidar mission. *Remote Sens. Environ.* **270**, 112845. https://doi.org/10.1016/j.rse.2021.112845 (2022).
33. Ni-Meister, W., Rojas, A. & Lee, S. Direct use of large-footprint lidar waveforms to estimate aboveground biomass. *Remote Sens. Environ.* **280**, 113147. https://doi.org/10.1016/j.rse.2022.113147 (2022).
34. Tian, Y. et al. Aboveground mangrove biomass estimation in Beibu Gulf using machine learning and UAV remote sensing. *Sci. Total Environ.* **781**, 146816. https://doi.org/10.1016/j.scitotenv.2021.146816 (2021).
35. Zhao, Y. et al. UAV-based individual shrub aboveground biomass estimation calibrated against terrestrial LiDAR in a shrub-encroached grassland. *Int. J. Appl. Earth Obs. Geoinf.* **101**, 102358. https://doi.org/10.1016/j.jag.2021.102358 (2021).
36. Fatoyinbo, T. et al. The NASA AfriSAR campaign: Airborne SAR and lidar measurements of tropical forest structure and biomass in support of current and future space missions. *Remote Sens. Environ.* **264**, 112533. https://doi.org/10.1016/j.rse.2021.112533 (2021).
37. Navarro, A. et al. The application of Unmanned Aerial Vehicles (UAVs) to estimate above-ground biomass of mangrove ecosystems. *Remote Sens. Environ.* **242**, 111747. https://doi.org/10.1016/j.rse.2020.111747 (2020).
38. Ma, L. et al. Spatial heterogeneity of global forest aboveground carbon stocks and fluxes constrained by spaceborne lidar data and mechanistic modeling. *Glob. Change Biol.* **29**, 3378–3394. https://doi.org/10.1111/gcb.16682 (2023).
39. Daniels, L. et al. Identifying the Optimal Radiometric Calibration Method for UAV-Based Multispectral Imaging. *Remote Sens.* **15**, 2909. https://doi.org/10.3390/rs15112909 (2023).
40. Shendryk, Y. et al. Fine-scale prediction of biomass and leaf nitrogen content in sugarcane using UAV LiDAR and multispectral imaging. *Int. J. Appl. Earth Obs. Geoinf.* **92**, 102177. https://doi.org/10.1016/j.jag.2020.102177 (2020).
41. Deyong, Y., Hongbo, S., Peijun, S., Wenquan, Z. & Yaozhong, P. How does the conversion of land cover to urban use affect net primary productivity? A case study in Shenzhen city. *China. Agric. For. Meteorol.* **149**, 2054–2060. https://doi.org/10.1016/j.agrformet.2009.07.012 (2009).
42. Wu, C. et al. Improved CASA model based on satellite remote sensing data: simulating net primary productivity of Qinghai Lake basin alpine grassland. *Geosci. Model Dev.* **15**, 6919–6933. https://doi.org/10.5194/gmd-15-6919-2022 (2022).
43. Potter, C. S. et al. Terrestrial ecosystem production: A process model based on global satellite and surface data. *Glob. Biogeochem. Cycle* **7**, 811–841. https://doi.org/10.1029/93GB02725 (1993).
44. Field, C. B., Randerson, J. T. & Malmström, C. M. Global net primary production: Combining ecology and remote sensing. *Remote Sens. Environ.* **51**, 74–88. https://doi.org/10.1016/0034-4257(94)00066-V (1995).
45. Potter, C. S. Terrestrial Biomass and the Effects of Deforestation on the Global Carbon Cycle: Results from a model of primary production using satellite observations. *Bioscience* **49**, 769–778. https://doi.org/10.2307/1313568 (1999).
46. Wang, N., Hou, W., Zhang, X., Wang, Z. & Yang, L. Quantifying the effects of the "Internet plus Ecology" framework on carbon sink in the digital age: a representative study of Ant Forest in China. *Environ. Res. Lett.* **17**, 124005. https://doi.org/10.1088/1748-9326/aca2bf (2022).
47. Chen, J., Shao, Z., Huang, X. & Hu, B. Multi-source data-driven estimation of urban net primary productivity: A case study of Wuhan. *Int. J. Appl. Earth Obs. Geoinf.* **127**, 103638. https://doi.org/10.1016/j.jag.2023.103638 (2024).
48. Yan, Y., Wu, C. & Wen, Y. Determining the impacts of climate change and urban expansion on net primary productivity using the spatio-temporal fusion of remote sensing data. *Ecol. Indic.* **127**, 107737. https://doi.org/10.1016/j.ecolind.2021.10773 (2021).
49. Yan, N. et al. Assessment of the grassland carrying capacity for winter-spring period in Mongolia. *Ecol. Indic.* **146**, 109868. https://doi.org/10.1016/j.ecolind.2023.109868 (2023).
50. Lin, J., Chen, D., Wu, W. & Liao, X. Estimating aboveground biomass of urban forest trees with dual-source UAV acquired point clouds. *Urban For. Urban Green.* **69**, 127521. https://doi.org/10.1016/j.ufug.2022.127521 (2022).
51. Peng, M., Han, W., Li, C., Yao, X. & Shao, G. Modeling the daytime net primary productivity of maize at the canopy scale based on UAV multispectral imagery and machine learning. *J. Clean. Prod.* **367**, 133041. https://doi.org/10.1016/j.jclepro.2022.133041 (2022).
52. Sinde-González, I. et al. Biomass estimation of pasture plots with multitemporal UAV-based photogrammetric surveys. *Int. J. Appl. Earth Obs. Geoinf.* **101**, 102355. https://doi.org/10.1016/j.jag.2021.102355 (2021).
53. Jiang, J., Johansen, K., Tu, Y.-H. & McCabe, M. F. Multi-sensor and multi-platform consistency and interoperability between UAV, Planet CubeSat, Sentinel-2, and Landsat reflectance data. *GISci. Remote Sens.* **59**, 936–958. https://doi.org/10.1080/15481603.2022.2083791 (2022).
54. Santoro, M. et al. The global forest above-ground biomass pool for 2010 estimated from high-resolution satellite observations. *Earth Syst. Sci. Data* **13**, 3927–3950. https://doi.org/10.5194/essd-13-3927-2021 (2021).

55. Wang, D. et al. Estimating aboveground biomass of the mangrove forests on northeast Hainan Island in China using an upscaling method from field plots, UAV-LiDAR data and Sentinel-2 imagery. *Int. J. Appl. Earth Obs. Geoinf.* **85**, 101986. https://doi.org/10.1016/j.jag.2019.101986 (2020).
56. NASA. *Observing in Infrared. NASA Earth Observatory* https://earthobservatory.nasa.gov/features/FalseColor/page5.php (2014).
57. Shi, X. et al. Effects of climate change and human activities on gross primary productivity in the Heihe River Basin. *China. Environ. Sci. Pollut. Res.* **30**, 4230–4244. https://doi.org/10.1007/s11356-022-22505-y (2023).
58. Yuan, Y., Tang, S., Zhang, J. & Guo, W. Quantifying the relationship between urban blue-green landscape spatial pattern and carbon sequestration: A case study of Nanjing's central city. *Ecol. Indic.* **154**, 110483. https://doi.org/10.1016/j.ecolind.2023.110483 (2023).
59. Yang, F., He, P., Ding, H. & Shi, Y. A Monthly High-Resolution Net Primary Productivity Dataset (30 m) of Qinghai Plateau From 1987 to 2021. *IEEE J. Sel. Top. Appl. Earth Obs. Remote Sens.* **16**, 8262–8273 (2023). https://doi.org/10.1109/JSTARS.2023.3312518
60. Ma, J. et al. Spatial-temporal consistency between gross primary productivity and solar-induced chlorophyll fluorescence of vegetation in China during 2007–2014. *Sci. Total Environ.* **639**, 1241–1253. https://doi.org/10.1016/j.scitotenv.2018.05.245 (2018).
61. Xu, F., Wang, X. & Li, L. NPP and Vegetation Carbon Sink Capacity Estimation of Urban Green Space Using the Optimized CASA Model: A Case Study of Five Chinese Cities. *Atmosphere* **14**, 1161. https://doi.org/10.3390/atmos14071161 (2023).
62. Yan, Y. et al. Assessing the impacts of urban sprawl on net primary productivity using fusion of Landsat and MODIS data. *Sci. Total Environ.* **613–614**, 1417–1429. https://doi.org/10.1016/j.scitotenv.2017.09.201 (2018).
63. Zhang, Y. et al. Consistency between sun-induced chlorophyll fluorescence and gross primary production of vegetation in North America. *Remote Sens. Environ.* **183**, 154–169. https://doi.org/10.1016/j.rse.2016.05.015 (2016).
64. Feng, Q., Liu, J. & Gong, J. UAV Remote Sensing for Urban Vegetation Mapping Using Random Forest and Texture Analysis. *Remote Sens.* **7**, 1074–1094. https://doi.org/10.3390/rs70101074 (2015).
65. Daryaei, A., Sohrabi, H., Atzberger, C. & Immitzer, M. Fine-scale detection of vegetation in semi-arid mountainous areas with focus on riparian landscapes using Sentinel-2 and UAV data. *Comput. Electron. Agric.* **177**, 105686. https://doi.org/10.1016/j.compag.2020.105686 (2020).
66. Nahrstedt, K., Reuter, T., Trautz, D., Waske, B. & Jarmer, T. Classifying Stand Compositions in Clover Grass Based on High-Resolution Multispectral UAV Images. *Remote Sens.* **16**, 1234 (2024).
67. Congalton, R. G. & Green, K. *Assessing the Accuracy of Remotely Sensed Data: Principles and Practices.* 3rd edn. CRC Press/Taylor & Francis (2019).
68. Jensen, J. R. *Introductory Digital Image Processing: A Remote Sensing Perspective.* 4th edn. Pearson (2015).
69. Campbell, J. B. & Wynne, R. H. *Introduction to Remote Sensing.* 5th edn. Guilford Press (2011).
70. Liu, Y. et al. Estimation of Terrestrial Net Primary Productivity in China from Fengyun-3D Satellite Data. *J. Meteorol. Res.* **36**, 401–416. https://doi.org/10.1007/s13351-022-1183-6 (2022).
71. Los, S. O. *Linkages Between Global Vegetation and Climate: An Analysis Based on NOAA Advanced Very High Resolution Radiometer Data*. (NASA Goddard Space Flight Center, 1998).
72. Huang, X. et al. An improved Carnegie-Ames-Stanford Approach model for estimating ecological carbon sequestration in mountain vegetation. *Front. Ecol. Evol.* **10**, 1048607. https://doi.org/10.3389/fevo.2022.1048607 (2022).
73. Xiao, X. et al. Satellite-based modeling of gross primary production in an evergreen needleleaf forest. *Remote Sens. Environ.* **89**, 519–534. https://doi.org/10.1016/j.rse.2003.11.008 (2004).
74. Lambers, H., Chapin, F. S. & Pons, T. L. *Ecosystem and Global Processes: Ecophysiological Controls in Plant Physiological Ecology* 555–571 (Springer, 2008).
75. Chave, J. et al. Improved allometric models to estimate the aboveground biomass of tropical trees. *Glob. Change Biol.* **20**, 3177–3190 (2014).

Author contributions

Chien-Hao Sung: Conceptualization, Data curation, Investigation, Methodology, Software, Validation, Visualization, Writing the original draft, Writing—review and editing of the manuscript. Candera Wijaya: Data curation, Methodology, Software. Aji Kusumaning Asri: Data curation, Visualization, Writing—review and editing of the manuscript. Yinq-Rong Chern: Data curation, Visualization, Writing—review and editing of the manuscript. Tee-Ann Teo: Methodology, Writing—review and editing of the manuscript. Wan-Yu Liu: Funding acquisition, Writing—review and editing of the manuscript. Chia-Ho Lee: Funding acquisition, Writing—review and editing of the manuscript. Yu-Liang Hsu: Funding acquisition, Writing—review and editing of the manuscript. Chih-Da Wu: Conceptualization, Funding acquisition, Methodology, Project administration, Supervision, Validation, Writing—review and editing of the manuscript.

Funding

This study was supported by the National Science and Technology Council, Taiwan (NSTC 113–2121-M-006–010 -; 114–2119-M-006 -010 -; 114–2123-M-001 -006 -; 114–2121-M-006 -001), and the Higher Education Sprout Project by the Ministry of Education (MOE) in Taiwan. This work was supported partially by the Research Center for Precision Environmental Medicine, Kaohsiung Medical University, Kaohsiung, Taiwan from The Featured Areas Research Center Program within the framework of the Higher Education Sprout Project by the Ministry of Education (MOE) in Taiwan and by Kaohsiung Medical University Research Center Grant (KMU-TC114A01). This research was also funded by the Chang Gung University of Science and Technology Foundation (ZRRPF6N0011), and Chang Gung Medical Research Program Foundation (CMRPF6P0041, CMRPF6P0042, and CMRPF6P0043).

Declarations

Competing interests

The authors declare that they have no known competing financial interests or personal relationships that could have appeared to influence the work reported in this paper.

Additional information

Correspondence and requests for materials should be addressed to C.-D.W.